Applied Physics Letters

RESEARCH ARTICLE | SEPTEMBER 13 2023

Hybrid integration of ensemble nitrogen-vacancy centers in single-crystal diamond based on pick-flip-and-place transfer printing

Ryota Katsumi ; Kosuke Takada ; Shun Naruse ; Kenta Kawai ; Daichi Sato ; Takeshi Hizawa; Takashi Yatsui

Appl. Phys. Lett. 123, 111108 (2023)
https://doi.org/10.1063/5.0161268

AIP Publishing

Applied Physics Letters ARTICLE pubs.aip.org/aip/apl

Hybrid integration of ensemble nitrogen-vacancy centers in single-crystal diamond based on pick-flip-and-place transfer printing

Cite as: Appl. Phys. Lett. **123**, 111108 (2023); doi: 10.1063/5.0161268
Submitted: 28 June 2023 · Accepted: 3 September 2023 ·
Published Online: 13 September 2023

Ryota Katsumi,[1,2,a] Kosuke Takada,[1] Shun Naruse,[1] Kenta Kawai,[1] Daichi Sato,[1] Takeshi Hizawa,[1] and Takashi Yatsui[1,2]

AFFILIATIONS

[1]Graduate School of Engineering, Toyohashi University of Technology, 1-1 Hibarigaoka, Tempaku-cho, Toyohashi, Aichi 441-8580, Japan
[2]Graduate School of Engineering, the University of Tokyo, 7-3-1 Hongo, Bunkyo-ku, Tokyo 113-8656, Japan

[a]Author to whom correspondence should be addressed: katsumi.ryota.ti@tut.jp

ABSTRACT

Incorporating color centers in diamond with mature integrated photonics using hybrid integration techniques such as transfer printing provides a promising route toward scalable quantum applications. However, single-crystal diamond nanostructures fabricated using current etching technologies have triangular bottoms that are unsuitable for conventional pick-and-place integration. Herein, we present an alternative approach for deterministically integrating diamond nanostructures on chip. We demonstrate the hybrid integration of a diamond triangular nanobeam containing a nitrogen-vacancy ensemble on an SiO_2 chip by picking it up using a weak adhesive film, flipping it, and transferring it to a stronger one. This "pick-flip-and-place" approach provides a flat diamond-chip interface, enabling the high-yield hybrid integration regardless of the shape of diamond nanostructures. Additionally, diamond nanofabrication is facilitated by transfer-printing hard masks for diamond etching. We also show that the integrated diamond nanobeam functions as a nanoscale quantum sensor. Our proposed approach paves the way toward scalable hybrid-diamond quantum photonics.

Color centers in single-crystal diamond have been explored for a wide variety of quantum technologies, including quantum sensing, quantum communication, and quantum computation.[1–3] Owing to the excellent properties of their electron spins with long coherence time at room temperature, nitrogen-vacancy (NV) centers in diamond are exploited for sensitive solid-state quantum sensors to detect various environmental parameters such as magnetic field,[4–6] electric field,[7] and temperature.[8,9] Because NV-based quantum sensors have been proven to offer pico-Tesla magnetic field sensitivity at room temperature,[10,11] they have been applied to various areas across condensed matter physics, geoscience, and biology.[12–16] The NV center is also promising candidates for solid-state quantum memories with second-scale spin coherence times.[17] Recent demonstrations have been reported on a laboratory-scale quantum network using three separate NV centers in diamonds, showcasing the potential of the color centers in diamonds as quantum network node candidates.[18]

To accelerate advances in diamond-based quantum technologies, it is important to implement micro/nanostructures in diamonds. Owing to recent advancements in diamond nanofabrication technologies, including the membrane-thinning approach,[19] angled etching,[20] quasi-isotropic etching,[21] and reactive ion-beam angled etching,[22] a wide variety of nanophotonic structures (e.g., photonic crystals,[19,23–27] photonic waveguides,[20,28] ring resonators,[23,29] grating structure,[30] and disk resonators[21,31]) have been demonstrated to date. A recent study employed a diamond nanocavity to demonstrate memory-enhanced quantum communication based on silicon-vacancy (SiV) centers.[32]

The next stage toward scalable diamond quantum photonics is the integration of diamond color centers on chips based on other materials, because the scalability of monolithic diamond photonics is limited by the lack of the technology to fabricate wafer-scale diamond photonic integrated circuits. Alternatively, the integration of NV centers onto well-developed photonic platforms, including Si, SiN, $LiNbO_3$, and AlN, is promising for building large-scale multifunctional quantum photonic integrated devices.[33] Meanwhile, the heteroepitaxial growth of high-quality single-crystal diamond thin films on different material platforms is challenging owing to the current diamond

growth technology.[34] A potential solution for hybrid integration of diamond on chip is the use of pick-and-place techniques,[33] which offer a viable route to combine color centers with state-of-the-art integrated photonics. Thus far, the hybrid integration of a diamond microwaveguide onto an SiN waveguide has been demonstrated using a micromanipulator.[35] Among the pick-and-place techniques, transfer printing is becoming widely adopted as a back-end process for the hybrid integration of prefabricated photonic and electronic devices at arbitrary locations of desirable materials.[36–44] However, the current nanofabrication technology for diamond photonics is inherently incompatible with existing hybrid integration approaches. For example, a diamond nanostructure fabricated using angled etching has a triangular bottom surface that is structurally difficult to place on other substrates using conventional pick-and-place techniques. Recently, the hybrid integration of an array of diamond waveguides containing germanium-vacancy (GeV) and SiV centers onto an AlN photonic chip has been achieved using a micromanipulator owing to the nearly flat bottom surface of the diamond waveguides fabricated through quasi-isotropic etching.[45] Nevertheless, the bottom of the diamond nanostructures formed through quasi-isotropic etching is non-flat, depending on their width and shape,[46] making it difficult to integrate them on chip using conventional pick-and-place approaches. Thus, the development of hybrid integration techniques with near-unity yields, regardless of the sample structure, is essential for scalable diamond quantum photonics. Notably, none have demonstrated the hybrid integration of a diamond nanobeam with an ensemble of NV centers on a chip for quantum sensing.

In this study, we demonstrate the hybrid integration of a diamond NV triangular nanobeam on chip in a deterministic manner. We propose pick-flip-and-place transfer printing, which picks up and flips a suitable diamond nanostructure using a weak adhesive film, transfers it to another strong one, and places it on a desirable photonics chip. This approach provides a flat interface between a diamond nanostructure and a photonic chip, enabling the integration of NV centers on chip with a near-unity success rate, regardless of the shape or width of the diamond nanostructures. We also demonstrate that transfer printing can be exploited to facilitate the fabrication of air-bridged nanostructures in a single-crystal diamond by integrating SiN nano-scale hard masks on the diamond for the diamond etching process. We experimentally demonstrate that an integrated diamond nanobeam containing an ensemble of NV centers can function as a nanoscale quantum sensor by performing detailed optical characterization and optically detected magnetic resonance (ODMR) measurements. The proposed approach is a key technology for the development of scalable diamond quantum photonics assisted by cutting-edge photonic technologies.

The basic procedure for the proposed nanofabrication and hybrid integration processes based on transfer printing is outlined in Figs. 1(a)–1(h). First, we prepared air-suspended hard-mask nanostructures that were robust to diamond etching [Fig. 1(a)]. These hard masks were picked and placed onto a single-crystal diamond using transfer printing with a transparent polydimethylsiloxane (PDMS) adhesive film [Fig. 1(b)]. An air-suspended diamond structure was formed by transferring the mask pattern onto the diamond substrate via vertical dry etching [Fig. 1(c)], followed by a diamond undercut process (e.g., angled etching and quasi-isotropic etching) [Fig. 1(d)]. There are several challenges in patterning single-crystal diamond substrates using lithographic techniques. For instance, spin coating a photoresist or e-beam (EB) resist on diamond, which is typically several millimeters or less in size, is technically difficult. In addition, the low electrical conductivity of diamond renders it unsuitable for EB lithography and requires additional conductive layers for precise patterning. As mentioned above, the proposed approach requires only the hybrid integration of a prefabricated array of hard masks on diamond and subsequent plasma etching,[47] largely simplifying the nanofabrication of materials whose fabrication technology is undeveloped.

We then used transfer printing to select a suitable diamond nanostructure from the processed diamond substrate using a PDMS film with weak adhesion, following the same procedure as that shown in Fig. 1(a) [Fig. 1(e)]. We flipped this "weak" PDMS and lifted off the nanostructure from the flipped film using a PDMS film with strong adhesion [Fig. 1(f)]. This operation guarantees a flat interface between

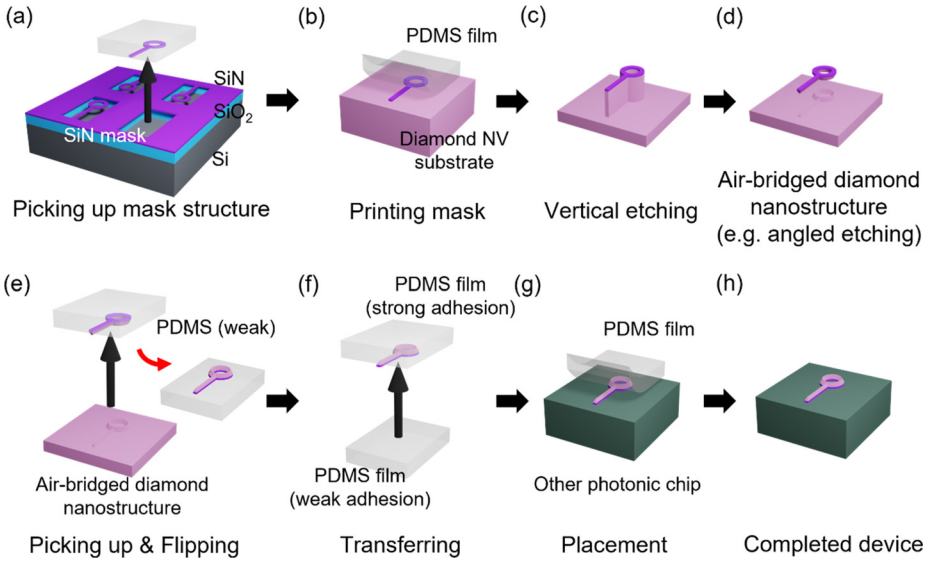

FIG. 1. Schematics of the proposed nanofabrication and integration process. (a) Picking-up air-suspended hard-mask nanostructures. (b) Printing hard masks onto a single-crystal diamond. (c) and (d) Air-suspended diamond structure that is formed by transferring the mask pattern onto the diamond substrate with vertical dry etching followed by diamond undercut. (e) Picking up a suitable diamond nanostructure from the diamond substrate using a PDMS film with weak adhesion. (f) Transferring the nanostructure from the weak flipped film to a PDMS film with strong adhesion. (g) Transferring diamond nanobeam onto another substrate. (h) Completed diamond structure integrated on chip.

the diamond nanostructures and photonic chip, which is necessary for high-yield integration. Finally, the transferred diamond nanobeam was integrated onto another substrate by slowly peeling off the film [Fig. 1(g)]. A schematic of the completed diamond structure integrated onto the chip is shown in Fig. 1(h). Notably, the proposed pick-flip-and-place integration approach enables hybrid integration regardless of the sample structure and target materials, expediting coordination between diamond quantum photonics and state-of-the-art photonic integration technology.

Figure 2(a) shows the structure of the device. A diamond nanobeam containing an ensemble of NV centers was placed on an SiO_2 substrate, which is commonly employed in integrated photonics as a low-refractive-index material to achieve efficient light confinement in a waveguide. The cross section of the nanobeam is an equilateral triangle, which is determined by the direction of the plasma during angled etching.[48] Because an NV center has two dipole orientations ($\boldsymbol{d}_1$ and $\boldsymbol{d}_2$), as shown in Fig. 2(b), a diamond waveguide should support both transverse electric (TE) and transverse magnetic (TM) polarizations for efficient waveguide coupling of the entire NV emission. We simulated the effective refractive-index dispersion of the waveguide modes at a wavelength of 637 nm using the finite element method. Here, we consider the typical refractive indices of diamond and SiO_2 to be 2.4 and 1.46, respectively. Figure 2(c) shows the dispersion of the investigated diamond waveguide as a function of the waveguide width. For widths ranging from 250 to 400 nm, the waveguide dispersion consisted of only the fundamental TE and TM modes. For widths $<$250 nm, the effective refractive index of the TE and TM modes was less than that of SiO_2, which caused low dipole-waveguide coupling owing to the weak light confinement in the waveguide. For a width $>$420 nm, waveguide dispersions of higher-order TE and TM modes

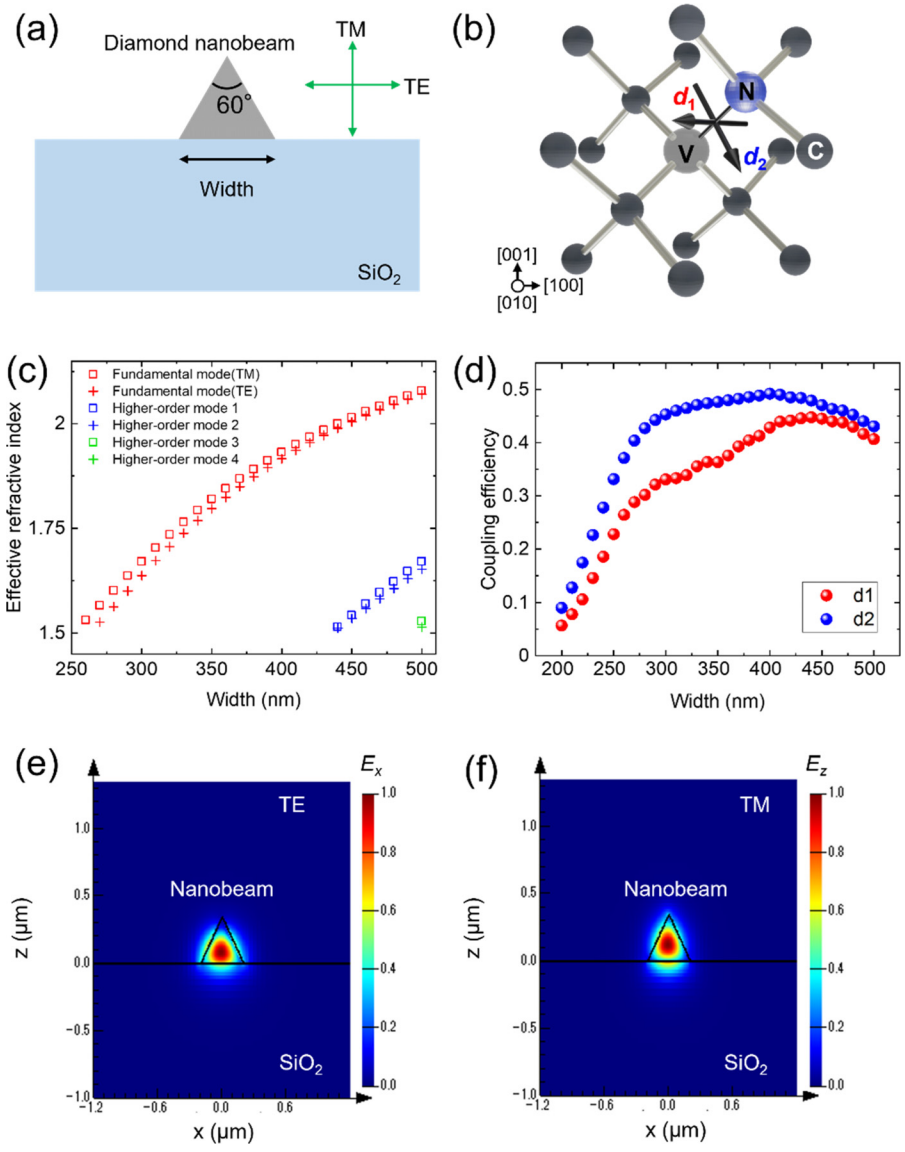

FIG. 2. (a) Schematics of the structure of the investigated device. (b) Two possible NV dipole orientations. (c) Dispersion of the investigated diamond waveguide as a function of the waveguide width. (d) Simulated NV dipole-waveguide coupling efficiency as a function of the waveguide width (red: $\boldsymbol{d}_1$; blue: $\boldsymbol{d}_2$). (e) and (f) field profiles of the TE mode and TM mode, respectively.

were observed, anticipating the undesirable loss of waveguide-coupled NV photons. We further simulated the coupling efficiency of the dipole emission from the NV center into the investigated waveguide using the finite-difference time-domain method. The red (blue) plots in Fig. 2(d) show the coupling efficiency of the dipole emissions of $\boldsymbol{d}_1$ ($\boldsymbol{d}_2$) into the investigated diamond nanobeam waveguide as a function of the waveguide width. The coupling efficiency is maximized around the width of approximately 400 nm for both dipole orientations, which agrees well with the results of the dispersion calculations.

To fabricate air-suspended diamond nanobeams, air-suspended SiN hard-mask structures were prepared. A 200-nm-thick low-pressure chemical vapor deposition (LPCVD) SiN layer was deposited on an SiO_2/Si substrate. A 100 nm-thick SiO_2 layer was used as a sacrificial layer to form an air-suspended SiN structure. The nanostructures were patterned with a polymer resist (ZEP520A) as a mask using EB lithography and dry etching processes. After removing the resist through an ashing process based on O_2 plasma, the structure was air-suspended through wet etching of the HF solution in 10 min, followed by drying in a critical point dryer to mitigate the capillary force. The etching selectivity of SiO_2/LPCVD SiN is over 100 in the current condition. Figure 3(a) shows an optical microscope image of the arrays of fabricated SiN hard masks. The SiN masks were suspended in a tether

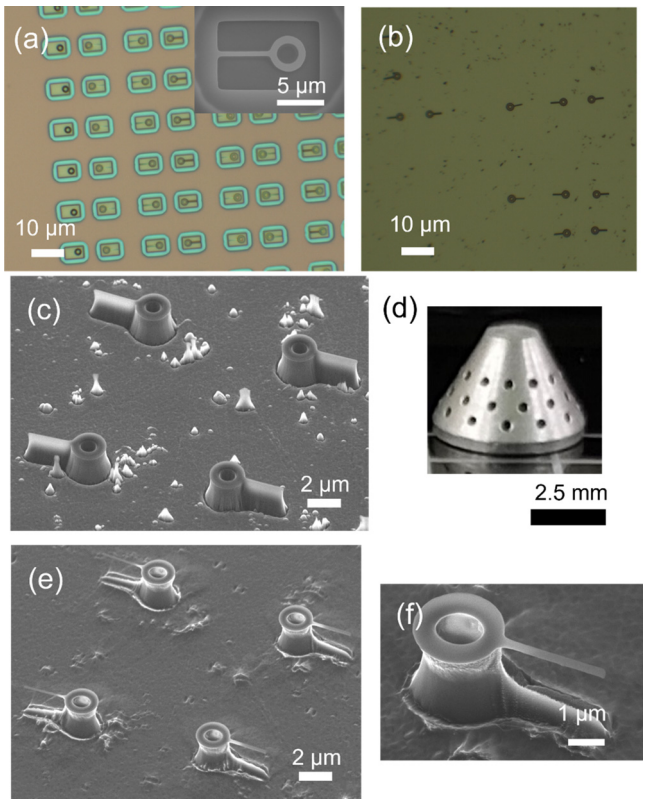

FIG. 3. (a) Optical microscope image of arrays of the fabricated SiN hard masks. Inset: SEM image of the SiN hard mask. (b) Optical microscope image of printed SiN masks. (c) SEM image of diamond nanostructures. (d) Photograph of the conical Faraday cage. (e) Bird's eye view of an SEM image of the air-suspended diamond nanobeam. (f) Magnified view of the fabricated device.

without any distortion. In parallel, we prepared a single-crystal type IIa diamond plate ($3 \times 3 \times 0.3\,mm^3$, Element Six) that were mechanically polished and cleaned with acetone.

Next, the fabricated SiN mask structure was transferred onto a single-crystal diamond plate. An adhesive thin film of PDMS (Sylgard184) was attached to a glass slide to monitor the samples using an optical microscope. The rubber film consists of two-part liquid components (a cross-linking curing agent and a pre-polymer base) that were mixed in 1:10 mass ratio. This mixture was then spin coated on a silicon wafer at 200 rpm for 5 s and 1000 rpm for 150 s. After the spin coating, the PDMS was baked at 100 °C for 5 min with an additional curing at 150 °C for 10 min using a hot plate. The film was laminated onto the suspended SiN mask structure and quickly removed [Fig. 1(a)]. The mask structure was printed onto a diamond surface with slow retraction, as shown in Fig. 1(b). Figure 3(b) shows an optical microscope image of the printed SiN masks. The arrays of mask structures were firmly bonded to the diamond surface through van der Waals forces. Results revealed that transfer printing enables the parallel integration of arrayed nano-scale hard masks,[40] which is important for the scalable fabrication of nanophotonic devices based on pick-and-place integration. The patterns of the printed masks were subsequently transferred to a diamond sample using O_2/Ar plasma dry etching (ULVAC ICP-RIE, 40 sccm O_2 gas flow, 2 sccm Ar gas flow, 1 Pa, and 1000 W power). Figure 3(c) shows a scanning electron microscopy (SEM) image of the diamond nanostructure. The mask patterns were transferred onto the diamond substrate. The sample was then placed inside a conical Faraday cage[49,50] [Fig. 3(d)] for undercutting using angled plasma etching under the same O_2/Ar plasma conditions. A Faraday cage was designed to achieve an etching angle of 60 °. Figures 3(e) and 3(f) show bird's eye and magnified views of the SEM images of the air-bridged diamond nanobeam, respectively. The width and angle of the fabricated diamond nanobeam were 280 nm and 60°, respectively. The slight derivation of the waveguide width from that in simulation (400 nm) is approximately due to the narrowing of the nanobeam during the angled etching. We emphasize that the proposed approach based on mask assembly of transfer printing does not require any other complicated processes for diamond, largely simplifying the nanofabrication of diamond photonics. Combining robotic automation[51,52] with transfer printing will further facilitate the fabrication of diamond-based quantum devices. We also note that the use of a PDMS film with a post array whose size and pitch match those of the mask array could enhance the transfer rate of SiN masks onto a target chip.[40]

Next, we performed pick-flip-and-place transfer printing to integrate a diamond nanobeam containing an ensemble of NV centers onto SiO_2. We patterned the diamond nanobeam structure on a diamond NV substrate with an NV density of 300 ppb ($3 \times 3 \times 0.5\,mm^3$, DNV-B1, Element Six), following the same procedure in Figs. 1(a)–(d). In general, high-density ensemble NV centers are formed by performing electron beam irradiation into a single-crystal diamond and subsequent annealing. For the target wafer, we deposited a 1-μm-thick SiO_2 layer onto the Si substrate. A PDMS film made from Sylgard184 was employed to pick up the diamond nanobeams. The pickup operation of the diamond nanobeam [Fig. 1(e)] is the same with Fig. 1(a). The PDMS film was then flipped by placing it on a sample stage. Figure 4(a) presents an optical microscopy image of the lifted diamond nanobeam on the flipped film. Subsequently, the diamond

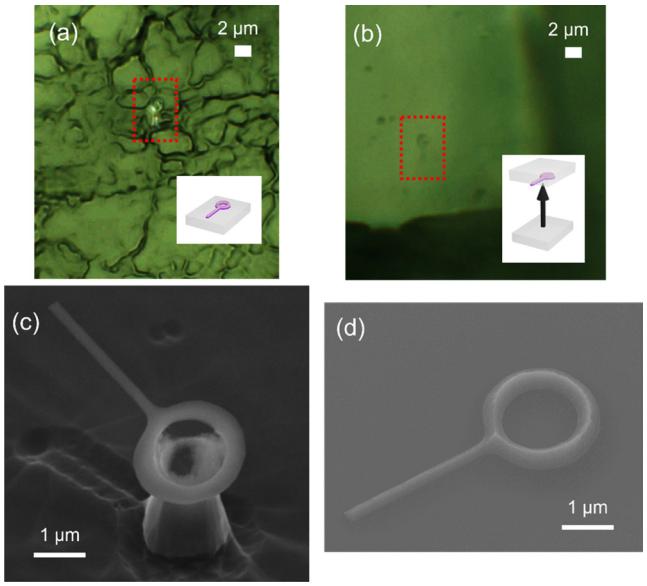

FIG. 4. (a) Optical microscope image of the lifted diamond nanobeam on a PDMS film with weak adhesion. (b) Optical microscope image of the transferred diamond nanobeam on a PDMS film with strong adhesion. (c) and (d) SEM images of the diamond nanobeam containing NV centers before and after the proposed hybrid integration, respectively.

nanobeam was transferred onto a commercial PDMS film with strong adhesion (PF-40 × 40-0065-X8, Gel-Pack). Figure 4(b) shows an optical microscope image of the transferred diamond nanobeam on the film with strong adhesion. We confirmed that this transfer process can be performed with a near-unity success rate. We also noted that the ring structure connected to the nanobeam prevented the attachment of the nanobeam's sidewalls onto the PDMS film during the flip process. Finally, the transferred diamond nanobeam was placed on the target SiO_2/Si substrate. Figures 4(c) and 4(d) show the SEM images of the diamond nanobeam containing NV centers before and after the proposed hybrid integration, respectively. The diamond nanobeam was flipped and firmly bonded to the chip, primarily through van der Waals forces. Notably, this printing process for triangular diamond nanobeams was performed with a success rate of over 80%. Although the surface roughness of SiN masks after the angled etching process is not investigated, smoother nanobeam-substrate interface can be achieved by removing the LPCVD SiN mask using hot phosphoric acid. The diamond surface with the roughness of less than 1 nm is routinely possible using mechanical polishing.[23] We consider that accurate integration of a diamond nanobeam onto a photonic waveguide is possible using the proposed pick-flip-and-place transfer printing owing to the precise positioning of transfer printing better than 100 nm.[37,41]

The fabricated device was characterized using micro-photoluminescence (μ-PL) spectroscopy. The integrated NV centers were optically excited using a continuous-wave laser oscillating at 532 nm. A ×100 objective lens with a numerical aperture of 0.8 was used to monitor the sample, irradiate the sample with an excitation laser beam, and collect the PL signals. To suppress the background light of the input laser, the PL signals from the NV centers were filtered using a notch filter (533 nm) and a long-pass filter (>600 nm). The background emission from the Si substrate was also filtered using a short-pass filter (<800 nm). The collected PL signals were analyzed using a grating spectrometer and a Si charge-coupled device (CCD) camera. Figure 5(a) shows the PL spectrum of the investigated sample. The spectrum exhibited only a strong peak of phonon-sideband emission (~720 nm) with a zero-phonon line (ZPL, 637 nm) and a negligible peak of the input laser (532 nm), confirming that the PL signal was dominated by the emission of the integrated NV centers. The weak ZPL peak is probably due to the relatively strong pump power.

Next, the pump-power dependence of the photon count rates was studied to evaluate the optical properties of the integrated diamond NV nanobeam. The collected PL signal was analyzed by switching the CCD camera to a single-photon avalanche detector. Figure 5(b) shows the measured photon count rate as a function of the pump power. The count rate (I) was determined using the following equation:

$$I = I_{\mathrm{sat}} \frac{P}{P + P_{\mathrm{sat}}} + I_{BG}, \tag{1}$$

where I_{sat} (I_{BG}) is the saturated (background) photon count rate and P (P_{sat}) is the input (saturation) laser power. In the current setup, we measured $I_{BG} \sim 1$ kilo count per second (kcps), which is negligible, compared to the photon count rate of the NV emission. Fitting the data obtained using Eq. (1) leads to $I_{\mathrm{sat}} = 2100$ kcps and $P_{sat} = \sim 60$ mW. Because ~600 NV centers in the diamond nanobeam contribute

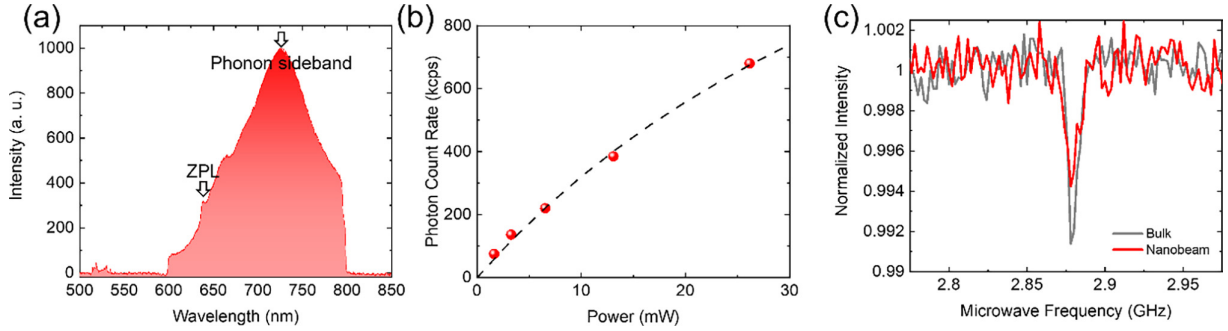

FIG. 5. (a) PL spectrum measured for the investigated sample. (b) Power dependence of photon count rate. Dotted line: fitting curve using Eq. (1). (c) ODMR spectrum for the investigated sample with no external magnetic field. Gray curve: typical ODMR spectrum measured for a bulk diamond NV substrate.

to the photon counts, the saturation power per NV center is ~100 μW. Compared to a previous study reporting P_{sat} of 250 μW for single NV center,[53] the obtained saturation power in this study was slightly lower, indicating the possibility of an efficient optical excitation of NV centers assisted by the nanobeam structure.

To demonstrate the potential of the integrated quantum sensor, we performed ODMR measurements on integrated NV centers. The NV center was microwave-excited using a thin copper film attached to the sample. Figure 5(c) shows the ODMR spectrum of the investigated sample with no external magnetic field and a pumping power of 7 mW. An ODMR dip exists at a microwave frequency of 2.88 GHz with an ODMR contrast of ~0.006. For comparison, the ODMR spectrum of the bulk diamond NV substrate is indicated by the gray curve in Fig. 5(c). By fitting these obtained data using the Lorenzian peak, the linewidth of the ODMR dip is deduced to be 7.8 (5.4) MHz for the integrated diamond nanobeam (bulk diamond). We attribute this slight linewidth broadening to the degraded coherence of the NV center stemming from the etched surface roughness, which can be improved by optical near-field-based surface etching.[54] We also note that the narrower linewidth of the ODMR spectrum could be achieved by employing pulsed ODMR measurement which coherently manipulates spins of NV centers.[53]

In conclusion, we demonstrated the hybrid integration of diamond triangle nanobeams on a chip using pick-flip-and-place transfer printing, which offers a flat diamond-chip interface and allows for the high-yield integration regardless of the shape and width of diamond nanostructures. We also demonstrated that transfer printing enables the introduction of SiN nano-scale hard masks for diamond etching, thereby facilitating the fabrication of air-bridged nanostructures in single-crystal diamond. We experimentally demonstrated that an integrated diamond nanobeam containing an ensemble of NV centers could function as a nanoscale quantum sensor. It is notable that the use of nanostructure for quantum sensing is beneficial for nanoscale spatial resolution, high sensitivity, and low power consumption.[55] The proposed approach based on transfer printing provides a deterministic route toward a scalable combination of diamond quantum photonics and cutting-edge integrated photonics technologies.

This work was supported by the MEXT Quantum Leap Flagship Program (MEXT Q-LEAP) (Grant No. JPMXS0118067395), KAKENHI (Nos. 20H02197, 20H05091, 20K21118, 21K20428, 22H01525, and 22K14289), and a research grant (Basic Research) from the TEPCO Memorial Foundation, Matsuo Foundation, and Murata Foundation.

AUTHOR DECLARATIONS

Conflict of Interest

The authors have no conflicts to disclose.

Author Contributions

Ryota Katsumi: Conceptualization (equal); Data curation (equal); Formal analysis (equal); Funding acquisition (equal); Investigation (equal); Methodology (equal); Project administration (equal); Resources (equal); Software (equal); Validation (equal); Visualization (equal); Writing – original draft (equal); Writing – review & editing (equal). **Kosuke Takada:** Methodology (equal); Resources (equal). **Shun Naruse:** Methodology (equal); Resources (equal). **Kenta Kawai:** Methodology (equal); Resources (equal). **Daichi Sato:** Methodology (equal); Resources (equal). **Takeshi Hizawa:** Methodology (equal); Resources (equal). **Takashi Yatsui:** Project administration (equal); Supervision (equal); Writing – review & editing (equal).

DATA AVAILABILITY

The data that support the findings of this study are available from the corresponding author upon reasonable request.

REFERENCES

[1]J. M. Taylor, P. Cappellaro, L. Childress, L. Jiang, D. Budker, P. R. Hemmer, A. Yacoby, R. Walsworth, and M. D. Lukin, Nat. Phys. **4**, 810 (2008).
[2]J. F. Barry, J. M. Schloss, E. Bauch, M. J. Turner, C. A. Hart, L. M. Pham, and R. L. Walsworth, Rev. Mod. Phys. **92**, 015004 (2020).
[3]M. Ruf, N. H. Wan, H. Choi, D. Englund, and R. Hanson, J. Appl. Phys. **130**, 070901 (2021).
[4]Y. Wu, F. Jelezko, M. B. Plenio, and T. Weil, Angew. Chem., Int. Ed. Engl. **55**, 6586 (2016).
[5]A. Kuwahata, T. Kitaizumi, K. Saichi, T. Sato, R. Igarashi, T. Ohshima, Y. Masuyama, T. Iwasaki, M. Hatano, F. Jelezko, M. Kusakabe, T. Yatsui, and M. Sekino, Sci. Rep. **10**, 2483 (2020).
[6]F. M. Stürner, A. Brenneis, T. Buck, J. Kassel, R. Rölver, T. Fuchs, A. Savitsky, D. Suter, J. Grimmel, S. Hengesbach, M. Förtsch, K. Nakamura, H. Sumiya, S. Onoda, J. Isoya, and F. Jelezko, Adv. Quantum Technol. **4**, 2000111 (2021).
[7]F. Dolde, H. Fedder, M. W. Doherty, T. Nöbauer, F. Rempp, G. Balasubramanian, T. Wolf, F. Reinhard, L. C. L. Hollenberg, F. Jelezko, and J. Wrachtrup, Nat. Phys. **7**, 459 (2011).
[8]G. Kucsko, P. C. Maurer, N. Y. Yao, M. Kubo, H. J. Noh, P. K. Lo, H. Park, and M. D. Lukin, Nature **500**, 54 (2013).
[9]M. Fujiwara, S. Sun, A. Dohms, Y. Nishimura, K. Suto, Y. Takezawa, K. Oshimi, L. Zhao, N. Sadzak, Y. Umehara, Y. Teki, N. Komatsu, O. Benson, Y. Shikano, and E. Kage-Nakadai, Sci. Adv. **6**, aba9636 (2020).
[10]T. Wolf, P. Neumann, K. Nakamura, H. Sumiya, T. Ohshima, J. Isoya, and J. Wrachtrup, Phys. Rev. X **5**, 041001 (2015).
[11]C. Zhang, F. Shagieva, M. Widmann, M. Kübler, V. Vorobyov, P. Kapitanova, E. Nenasheva, R. Corkill, O. Rhrle, K. Nakamura, H. Sumiya, S. Onoda, J. Isoya, and J. Wrachtrup, Phys. Rev. Appl. **15**, 064075 (2021).
[12]S. C. Scholten, A. J. Healey, I. O. Robertson, G. J. Abrahams, D. A. Broadway, and J. P. Tetienne, J. Appl. Phys. **130**, 150902 (2021).
[13]Y. Xie, A. T. Pierce, J. M. Park, D. E. Parker, E. Khalaf, P. Ledwith, Y. Cao, S. H. Lee, S. Chen, P. R. Forrester, K. Watanabe, T. Taniguchi, A. Vishwanath, P. Jarillo-Herrero, and A. Yacoby, Nature **600**, 439 (2021).
[14]D. R. Glenn, R. R. Fu, P. Kehayias, D. Le Sage, E. A. Lima, B. P. Weiss, and R. L. Walsworth, Geochem. Geophys. Geosyst. **18**, 3254 (2017).
[15]K. Arai, A. Kuwahata, D. Nishitani, I. Fujisaki, R. Matsuki, Y. Nishio, Z. Xin, X. Cao, Y. Hatano, S. Onoda, C. Shinei, M. Miyakawa, T. Taniguchi, M. Yamazaki, T. Teraji, T. Ohshima, M. Hatano, M. Sekino, and T. Iwasaki, Commun. Phys. **5**, 200 (2022).
[16]T. F. Segawa and R. Igarashi, Prog. Nucl. Magn. Reson. Spectrosc. **134–135**, 20 (2023).
[17]P. C. Maurer, G. Kucsko, C. Latta, L. Jiang, N. Y. Yao, S. D. Bennett, F. Pastawski, D. Hunger, N. Chisholm, M. Markham, D. J. Twitchen, J. I. Cirac, and M. D. Lukin, Science **336**, 1283 (2012).
[18]M. Pompili, S. L. N. Hermans, S. Baier, H. K. C. Beukers, P. C. Humphreys, R. N. Schouten, R. F. L. Vermeulen, M. J. Tiggelman, L. Dos Santos Martins, B. Dirkse, S. Wehner, and R. Hanson, Science **372**, 259 (2021).
[19]L. Li, T. Schroder, E. H. Chen, M. Walsh, I. Bayn, J. Goldstein, O. Gaathon, M. E. Trusheim, M. Lu, J. Mower, M. Cotlet, M. L. Markham, D. J. Twitchen, and D. Englund, Nat. Commun. **6**, 6173 (2015).
[20]M. J. Burek, N. P. de Leon, B. J. Shields, B. J. Hausmann, Y. Chu, Q. Quan, A. S. Zibrov, H. Park, M. D. Lukin, and M. Loncar, Nano Lett. **12**, 6084 (2012).
[21]B. Khanaliloo, M. Mitchell, A. C. Hryciw, and P. E. Barclay, Nano Lett. **15**, 5131 (2015).

[22]C. Chia, B. Machielse, A. Shams-Ansari, and M. Lončar, Opt. Express **30**, 14189 (2022).
[23]M. J. Burek, Y. Chu, M. S. Liddy, P. Patel, J. Rochman, S. Meesala, W. Hong, Q. Quan, M. D. Lukin, and M. Loncar, Nat. Commun. **5**, 5718 (2014).
[24]S. Mouradian, N. H. Wan, T. Schröder, and D. Englund, Appl. Phys. Lett. **111**, 021103 (2017).
[25]K. Kuruma, B. Pingault, C. Chia, D. Renaud, P. Hoffmann, S. Iwamoto, C. Ronning, and M. Lončar, Appl. Phys. Lett. **118**, 230601 (2021).
[26]K. Kuruma, A. H. Piracha, D. Renaud, C. Chia, N. Sinclair, A. Nadarajah, A. Stacey, S. Prawer, and M. Lončar, Appl. Phys. Lett. **119**, 171106 (2021).
[27]A. E. Rugar, S. Aghaeimeibodi, D. Riedel, C. Dory, H. Lu, P. J. McQuade, Z.-X. Shen, N. A. Melosh, and J. Vučković, Phys. Rev. X **11**, 031021 (2021).
[28]B. Machielse, S. Bogdanovic, S. Meesala, S. Gauthier, M. J. Burek, G. Joe, M. Chalupnik, Y. I. Sohn, J. Holzgrafe, R. E. Evans, C. Chia, H. Atikian, M. K. Bhaskar, D. D. Sukachev, L. Shao, S. Maity, M. D. Lukin, and M. Lončar, Phys. Rev. X **9**, 031022 (2019).
[29]A. Faraon, P. E. Barclay, C. Santori, K.-M. C. Fu, and R. G. Beausoleil, Nat. Photonics **5**, 301 (2011).
[30]L. Li, E. H. Chen, J. Zheng, S. L. Mouradian, F. Dolde, T. Schroder, S. Karaveli, M. L. Markham, D. J. Twitchen, and D. Englund, Nano Lett. **15**, 1493 (2015).
[31]M. Mitchell, D. P. Lake, and P. E. Barclay, APL Photonics **4**, 016101 (2019).
[32]M. K. Bhaskar, R. Riedinger, B. Machielse, D. S. Levonian, C. T. Nguyen, E. N. Knall, H. Park, D. Englund, M. Loncar, D. D. Sukachev, and M. D. Lukin, Nature **580**, 60 (2020).
[33]A. W. Elshaari, W. Pernice, K. Srinivasan, O. Benson, and V. Zwiller, Nat. Photonics **14**, 285 (2020).
[34]M. Schreck, S. Gsell, R. Brescia, and M. Fischer, Sci. Rep. **7**, 44462 (2017).
[35]S. L. Mouradian, T. Schröder, C. B. Poitras, L. Li, J. Goldstein, E. H. Chen, M. Walsh, J. Cardenas, M. L. Markham, D. J. Twitchen, M. Lipson, and D. Englund, Phys. Rev. X **5**, 031009 (2015).
[36]J. Lee, I. Karnadi, J. T. Kim, Y.-H. Lee, and M.-K. Kim, ACS Photonics **4**, 2117 (2017).
[37]R. Katsumi, Y. Ota, M. Kakuda, S. Iwamoto, and Y. Arakawa, Optica **5**, 691 (2018).
[38]A. Osada, Y. Ota, R. Katsumi, M. Kakuda, S. Iwamoto, and Y. Arakawa, Phys. Rev. Appl. **11**, 024071 (2019).
[39]R. Katsumi, Y. Ota, A. Osada, T. Yamaguchi, T. Tajiri, M. Kakuda, S. Iwamoto, H. Akiyama, and Y. Arakawa, APL Photonics **4**, 036105 (2019).
[40]J. Zhang, G. Muliuk, J. Juvert, S. Kumari, J. Goyvaerts, B. Haq, C. Op de Beeck, B. Kuyken, G. Morthier, D. Van Thourhout, R. Baets, G. Lepage, P. Verheyen, J. Van Campenhout, A. Gocalinska, J. O'Callaghan, E. Pelucchi, K. Thomas, B. Corbett, A. J. Trindade, and G. Roelkens, APL Photonics **4**, 110803 (2019).
[41]R. Katsumi, Y. Ota, T. Tajiri, M. Kakuda, S. Iwamoto, H. Akiyama, and Y. Arakawa, Opt. Express **29**, 37117 (2021).
[42]J. A. Smith, D. Jevtics, B. Guilhabert, M. D. Dawson, and M. J. Strain, Appl. Phys. Rev. **9**, 041317 (2022).
[43]R. Katsumi, T. Hizawa, A. Kuwahata, S. Naruse, Y. Hatano, T. Iwasaki, M. Hatano, F. Jelezko, S. Onoda, T. Ohshima, M. Sekino, and T. Yatsui, Appl. Phys. Lett. **121**, 161103 (2022).
[44]T.-W. Lu, Y.-C. Lin, and P.-T. Lee, ACS Photonics **10**, 2679 (2023).
[45]N. H. Wan, T. J. Lu, K. C. Chen, M. P. Walsh, M. E. Trusheim, L. De Santis, E. A. Bersin, I. B. Harris, S. L. Mouradian, I. R. Christen, E. S. Bielejec, and D. Englund, Nature **583**, 226 (2020).
[46]B. Khanaliloo, H. Jayakumar, A. C. Hryciw, D. P. Lake, H. Kaviani, and P. E. Barclay, Phys. Rev. X **5**, 041051 (2015).
[47]L. Li, I. Bayn, M. Lu, C. Y. Nam, T. Schroder, A. Stein, N. C. Harris, and D. Englund, Sci. Rep. **5**, 7802 (2015).
[48]P. Latawiec, M. J. Burek, Y.-I. Sohn, and M. Lončar, J. Vac. Sci. Technol. B **34**, 041801 (2016).
[49]S.-W. Jeon, J. Lee, H. Jung, S.-W. Han, Y.-W. Cho, Y.-S. Kim, H.-T. Lim, Y. Kim, M. Niethammer, W. C. Lim, J. Song, S. Onoda, T. Ohshima, R. Reuter, A. Denisenko, J. Wrachtrup, and S.-Y. Lee, ACS Photonics **7**, 2739 (2020).
[50]O. Cranwell Schaeper, J. E. Fröch, S. Kim, Z. Mu, M. Toth, W. Gao, and I. Aharonovich, Adv. Mater. Technol. **6**, 2100589 (2021).
[51]S. Masubuchi, M. Morimoto, S. Morikawa, M. Onodera, Y. Asakawa, K. Watanabe, T. Taniguchi, and T. Machida, Nat. Commun. **9**, 1413 (2018).
[52]J. McPhillimy, D. Jevtics, B. J. E. Guilhabert, C. Klitis, A. Hurtado, M. Sorel, M. D. Dawson, and M. J. Strain, ACS Appl. Nano Mater. **3**, 10326 (2020).
[53]A. Dréau, M. Lesik, L. Rondin, P. Spinicelli, O. Arcizet, J. F. Roch, and V. Jacques, Phys. Rev. B **84**, 195204 (2011).
[54]F. Brandenburg, R. Nagumo, K. Saichi, K. Tahara, T. Iwasaki, M. Hatano, F. Jelezko, R. Igarashi, and T. Yatsui, Sci. Rep. **8**, 15847 (2018).
[55]R. Katsumi, M. Sekino, and T. Yatsui, Jpn. J. Appl. Phys., Part 1 **61**, 082004 (2022).